THE JOURNAL OF PHYSICAL CHEMISTRY C

Article

Cite This: J. Phys. Chem. C 2019, 123, 9343−9351

pubs.acs.org/JPCC

Enhancement of the Spontaneous Emission Rate of Perovskite Nanowires Coupled into Cylindrical Hollow Nanocavities Formed on the Surface of Polystyrene Microfibers

Belkıs Gökbulut,[†] Arda Inanç,[†] Gokhan Topcu,[‡] Tugrul Guner,[‡] Mustafa M. Demir,[‡] and M. Naci Inci*[,†]

[†]Department of Physics, Bogazici University, Bebek, 34342 Istanbul, Turkey

[‡]Department of Materials Science and Engineering, Izmir Institute Technology, 35430 Izmir, Turkey

ABSTRACT: Fluorescent $CsPbBr_3$ nanowires are uniformly integrated into a porous polystyrene matrix in the form of microfibers to investigate the changes in their spontaneous emission rate. Cylindrical hollow nanocavities, ranging from 75 to 160 nm in diameter, are grown on the surface of the polymer microfibers during the fabrication process, which allow coupling light that is emitted from the excited $CsPbBr_3$ nanowires. Time-resolved experiments elucidate that the spontaneous emission rate of the perovskite nanowires is observed to increase by a factor of 4.9, upon coupling of the excited optical modes into the nanocavities, which is demonstrated to be in good agreement with our theoretical calculations.

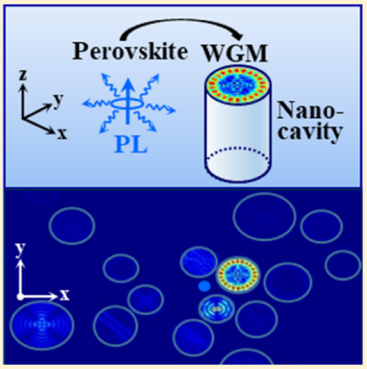

INTRODUCTION

Confinement of quantum emitters in nanostructures is one of the fundamental issues in cavity quantum electrodynamics if one aims to explain light−matter interactions deeply and also have a control over the spontaneous emission rate of a quantum emitter. The ability to intensify the electromagnetic waves in a subwavelength region alters the emission dynamics of the confined light emitters through modifications of the local density of the optical states in a surrounding medium. This revolutionary concept has opened novel avenues for dynamic controlling of light emitting quantum optical devices.[1,2] One of the main functions of the photonic nanostructures is to have the capability of enhancing the photon-radiation efficiency and the spontaneous emission rate of quantum light emitters, which offer an opportunity to improve the optical response of photonic devices, such as single photon sources,[3] nanolasers,[4] and solar cells.[5] Significant enhancement factors in the spontaneous emission rate have been demonstrated in many previous studies when the photonic environment is a resonator, which is tuned to the emission frequency of an ideal emitter, causing a modification in the vacuum field intensity and spectral density of the resonator's optical modes.[6−10] Although the resonator-induced ability to increase the spontaneous emission rate of a quantum emitter has attracted much interest, the reverse has also been well established in some elegant photonic environments with a decreased localized density of optical states.[11−13]

Various nano- or microstructures, such as whispering gallery-type microresonators,[14,15] periodically structured photonic crystals with defect modes,[16] and high-index contrast micro-pillar cavities based on the Bragg reflectors[17] are employed to alter the spontaneous emission rate of the confined emitters, such as quantum dots, nanowires (NWs), or organic fluorescent molecules. However, the majority of these host nanostructures are quite sophisticated, which require advanced engineering designs and costly production processes. Polymer-based nano- or micro fibers, which are doped with quantum emitters, have become favored alternatives as stable and reproducible photonic structures for controlling the spontaneous emission rate of the excited light emitters.[18] In this paper, hollow nanocylindrical cavities of diameters ranging from 75 to 160 nm are formed on the surface of the electrospun polystyrene (PS) microfibers to allow coupling of the light emission from perovskite NWs that are embedded within the microfibers. Thus, surface morphology of the polymer fiber, which depends on the electrospinning parameters during their production process, provides randomly distributed unique nanostructures to alter spontaneous emission rate of the emitters. The physical mechanism that alters the spontaneous emission rate of the confined perovskite NWs is analyzed using a time-resolved fluorescence lifetime spectroscopic method. The photonic design of the cylindrical hollow nanocavities allows supporting whispering gallery modes (WGMs) because of the total internal reflection at the boundary between air holes and the polymer matrix. When the NWs emit fluorescence near the hollow nanocavities, the

Received: December 17, 2018
Revised: March 13, 2019
Published: March 13, 2019

DOI: 10.1021/acs.jpcc.8b12114
J. Phys. Chem. C 2019, 123, 9343−9351

radiation from the excited emitters is coupled into the WGM. The spontaneous emission rate of the perovskite NWs is measured and found to be enhanced by a factor of 4.9, which is in good agreement with the average theoretical value of 4.7.

Perovskite nanocrystals have attracted much interest over a decade because of their exceptional photovoltaic assets[19,20] and noteworthy intrinsic features, such as strong absorption coefficient, high photoluminescence yield at room temperature, high charge carrier mobility and stability, and long nonradiative decay paths.[21−23] These nanomaterials have a favorable combination of quantum-size effects, which enhance their optical characteristics significantly with respect to their bulk counterparts. One can easily adjust the dimensions of these semiconductors through their inorganic material compositions during their growth processes to have a control over their photophysical properties, for example, tuning their emission wavelength from ultraviolet to near-infrared.[24] In 1D perovskite NWs, the stability of excitons is observed to immensely enhance due to the attracting quasi-particles being confined.[25] In another work, high performance photodetectors were successfully built using ultralong and well-aligned perovskite NWs that yield a strong light emission and remarkable waveguiding.[26] Additionally, confinement of light emission from a semiconductor NW to a photonic nanostructure is practiced to advance the efficiency of an emitter because of a strong light−matter interaction.[27] High-performance multiphoton pumped lasing is also accomplished when the perovskite nanorods are served as photonic cavities with a high-gain medium to enhance the emission dynamics of the nanorods.[28] Furthermore, as demonstrated in this work, allowing the employment of perovskite nanocrystals into a variety of matrices promotes them to be indispensable nominees for being desired elements for lightwave devices, ranging from light emitting diodes to micro-/nanoscale lasers.[29,30]

THEORY

Spontaneous emission rate enhancement of an optical emitter in a photonic cavity because of coupling between the radiating dipole and its electromagnetic field has been lucidly expressed by the Purcell factor F_P[31]

$$F_P = \frac{3Q(\lambda_c/n)^3}{4\pi^2 V} \quad (1)$$

where λ_c is the central wavelength of the cavity mode, n is the refractive index, and Q is the quality factor of the cavity mode, which is defined as $Q = \lambda_c/\Delta\lambda_c$, if the emitter linewidth is assumed to be much narrower than the linewidth of the cavity mode. For the situations for which the emitter linewidth is much broader than the cavity linewidth, the quality factor is determined to be $Q = \lambda_c/\Delta\lambda_{em}$.[32] V is the effective mode volume, which is defined by integrating the electric field intensity over the volume in concern and normalizing it to the maximum electric field intensity[33]

$$V = \frac{\int \varepsilon(\vec{r})|E(\vec{r})|^2 dV}{\varepsilon_m(\vec{r})|E_m(\vec{r})|^2} \quad (2)$$

Thus, the spontaneous emission rate is significantly enhanced using cavities with a high quality factor and a small mode volume. In this work, hollow nanocylinders embedded on the surface of the polymer microfibers, in which perovskite NWs are uniformly distributed, offer an alternative for nanocavities with a small mode volume.

The schematic illustration of light coupling from fluorescing perovskite NWs into cylindrical hollow nanocavities is given in details in Figure 1. The cylindrical hollow nanocavities are

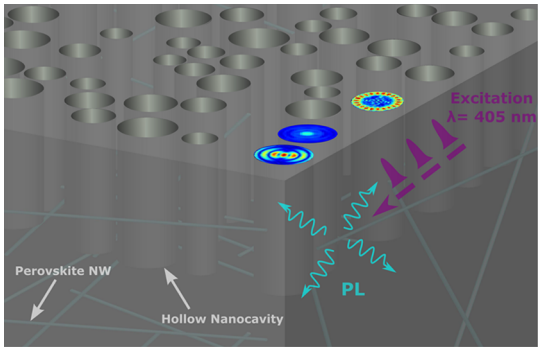

Figure 1. Schematic representation of the cylindrical hollow nanocavities on the surface of a PS microfiber and the excitation of the perovskite NWs embedded in it, which shows the coupling mechanism between the perovskite NWs and nanocylinders.

present on the surface of a PS microfiber, and the perovskite NWs are embedded further down in the same geometry. When the NWs are excited inside the microfiber by a laser beam with a wavelength of 405 nm, the emission from the excited NWs near the nanocylinders is coupled into the cavities, forming WGMs. As illustrated in Figure 2a, a single perovskite dipole is

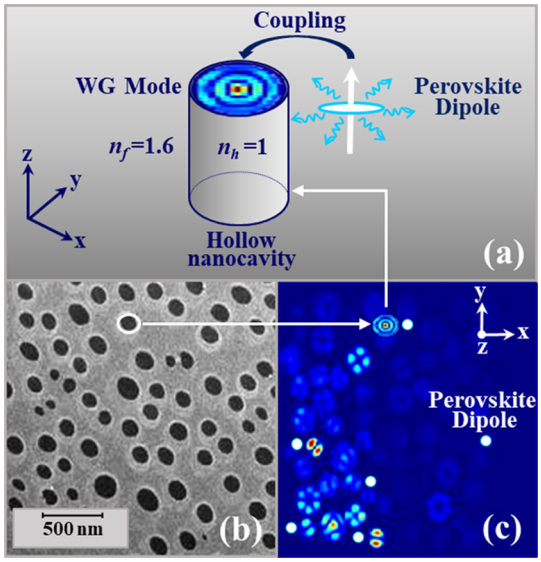

Figure 2. (a) Schematic representation of light coupling into a hollow nanocylindrical cavity from a radiating perovskite dipole. (b) Top view SEM image of the cylindrical hollow nanocavities (c) FDTD calculations of the electric field distribution that appears to be in the form of the WGM over the surface of an electrospun porous microfiber.

shown to couple a single cylindrical nanocavity, forming a WGM because of the total internal reflection at the boundary between the hollow nanocavity with a refractive index of $n_h = 1$ and the PS fiber with a refractive index of $n_f = 1.6$. Figure 2b shows the top view of a scanning electron microscopy (SEM) image of the cylindrical hollow nanocavities together with

DOI: 10.1021/acs.jpcc.8b12114
J. Phys. Chem. C 2019, 123, 9343−9351

finite difference time domain (FDTD) calculations of the electric field distribution that appears to be in the form of WGMs over the surface of an electrospun porous microfiber, as seen in Figure 2c.

Although the light confinement improves the efficiency of the 1D perovskite NWs, their spectral and spatial mismatches with respect to the corresponding cavity mode cause a reduction in the Purcell factor. As each NW experiences a distinctive spectral and spatial alignment with the WGM in concern, each emitter has a specific enhancement factor. Therefore, the total enhanced spontaneous emission rate requires being defined with some additional terms, beside the Purcell factor, as described in eq 3.[34] The ratio of the spontaneous emission rate of the NWs in a cavity (Γ) and bulk (Γ_0) is given as

$$\frac{\Gamma}{\Gamma_0} = F_p \frac{\Delta\lambda_c^{\,2}}{4(\lambda - \lambda_c)^2 + \Delta\lambda_c^{\,2}} \frac{|E(\vec{r})|^2}{|E_m|^2} 2\eta^2 \quad (3)$$

where $\Delta\lambda_c$ is the spectral linewidth of the cavity mode and $E(r)$ is the electric field amplitude of the WGMs with respect to the location of the NWs, in which the maximum electric field is given by $E_m = (h\nu/2\varepsilon_0 n^2 V)^{1/2}$. The second and the third terms represent spectral and spatial mismatch of the NW and the WGM, respectively. Spectral averaging of the second term results in a factor of 1/2, the average value of the third term is also determined to be approximately 1/3 for uniformly distributed NWs, η symbolizes the orientation matching of the dipole of the NW with respect to the polarization of the cavity mode, being equal to 1/3 for the case of randomly oriented dipoles of the NW, and factor of 2 originates from the two-fold degeneracy of the WGM, making eq 3 to be approximately 10 times smaller than eq 1,[35] which seems to describe the experimental results well.

EXPERIMENTAL SECTION

Material. Cesium carbonate (Cs_2CO_3, 99.9%, Sigma-Aldrich), lead(II) bromide ($PbBr_2$, ≥98%, Sigma-Aldrich), oleic acid (OA, 90%, Alfa Aesar), oleylamine (OAm, 90%, Sigma-Aldrich), 1-octadecene (ODE, 90%, Sigma-Aldrich), acetone (Merck, ≥99.5%), chloroform (≥99%, Sigma-Aldrich), tetrahydrofuran (THF, VWR, ≥99.7%), toluene (≥99%, Merck), and PS (M_w: 450 kg/mol, Sigma-Aldrich) were purchased and used as received without any further purification. The deionized water (18.2 MΩ·cm^{-1} at 25 °C) used in extraction was produced by a Milli-Q Advantage water treatment system.

Synthesis of Perovskite NWs. SEM image of the perovskite NWs produced and used in our experiments is demonstrated in Figure 3. The average diameter and length of the nanocrystals are determined to be 19 and 500 nm, respectively. $CsPbBr_3$ NWs are prepared using room-temperature crystallization with slight modifications based on the procedure given in ref 25. First, Cs oleate synthesis is carried out by dissolving Cs_2CO_3 (0.2 g) and OA (0.625 mL) in ODE (7.5 mL). The mixture is loaded into a container and dried under vacuum (150 mbar) at 120 °C for 1 h. Subsequently, the mixture is heated to 150 °C under N_2, and the reaction is maintained until all Cs_2CO_3 is consumed by OA.

For crystallization, an aliquot of OA (0.125 mL), OAm (0.125 mL), and ODE (1.25 mL) are loaded into a glass vial. Subsequently, 0.1 mL of preheated Cs oleate solution is added to the mixture. The third step involves the addition of 0.2 mL of $PbBr_2$ precursor solution (0.4 M, heated for 1 h at 80 °C until full dissolution). Finally, 5 mL of acetone is rapidly added to trigger the crystallization of the $CsPbBr_3$ NWs. Stirring is maintained for 30 min, and green precipitates are collected using a centrifuge (6000 rpm, 10 m). The precipitates are redispersed in toluene and the concentration is fixed to 10 mg/mL. Photoluminescence excitation (PLE) and emission (PL) spectra and X-ray diffraction (XRD) pattern of $CsPbBr_3$ NWs are given in Figure 4a,b, respectively.

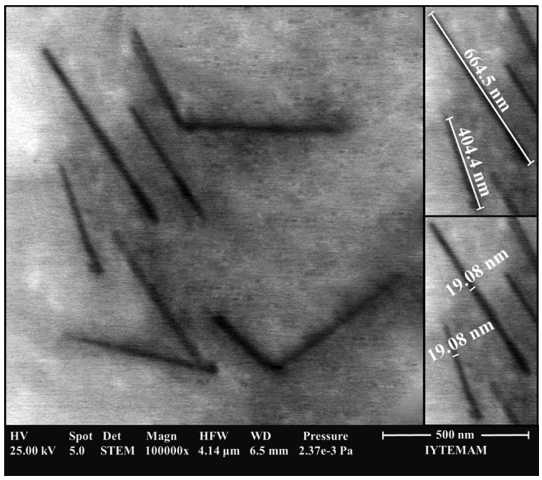

Figure 3. SEM images of $CsPbBr_3$ NWs.

Fabrication of NW-Doped PS Porous Microfibers. $CsPbBr_3$ NWs are embedded into a polymeric matrix via the electrospinning technique. The suspension mixture of $CsPbBr_3$ NWs and PS (30% w/v in THF) is subjected to high electrical field to form microfibers onto an aluminum foil collector. Two electrode holders are connected to the syringe needle and the collector, respectively. A fixed potential of 15 kV is applied, and the flow rate is set to 1 mL/h. Upon applied voltage, the polymer solution is ejected from the nozzle as a jet, overcoming surface tension of the droplet, forming fibers due to both solvent evaporation and continuous electrical force stretching. The formation of surface porosity of the PS fibers may originate from sequential evaporation of cosolvents during the electrospinning process.[36] The cosolvents of PS (THF, chloroform, and toluene) undergo liquid−liquid phase separation. Rapid evaporation of the most volatile solvent, which is chloroform in this mixture, may leave behind nanometric-sized pores on the surface of the electrospun fibers. SEM images of the porous fibers at different scales; 10, 2, and 1 μm are shown in Figure 5a−c, respectively. The diameters of the individual microfibers are determined to be approximately 10 and 13 μm, as seen in Figure 4a, although much smaller diameters around 3 μm are also observed within the microfiber mesh. The diameters of the cylindrical nanocavities are measured to range from 75 to 160 nm, as seen in Figure 5c. In a previous study,[37] field emission SEM and atomic force microscopy images allowed characterizing the pores, that is, the hollow cylindrical nanocavities, on the outer surface of the PS microfibers. Using determined parameter yields, the statistical average value of the pore depth is found to be approximately 50 nm.

Time-Resolved Fluorescence Lifetime Measurements. Time-resolved experiments are performed to examine fluorescence lifetime of nanorods confined in microfibers as depicted in Figure 6. A TimeHarp 200 PC-Board system

DOI: 10.1021/acs.jpcc.8b12114
J. Phys. Chem. C 2019, 123, 9343−9351

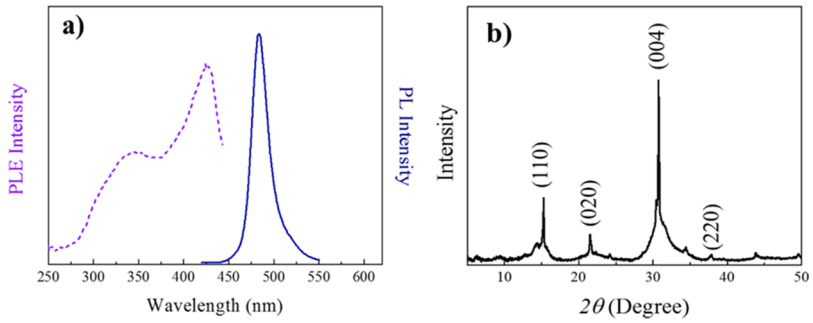

Figure 4. (a) Photoluminescence excitation and emission spectra and (b) XRD pattern of $CsPbBr_3$ NWs.

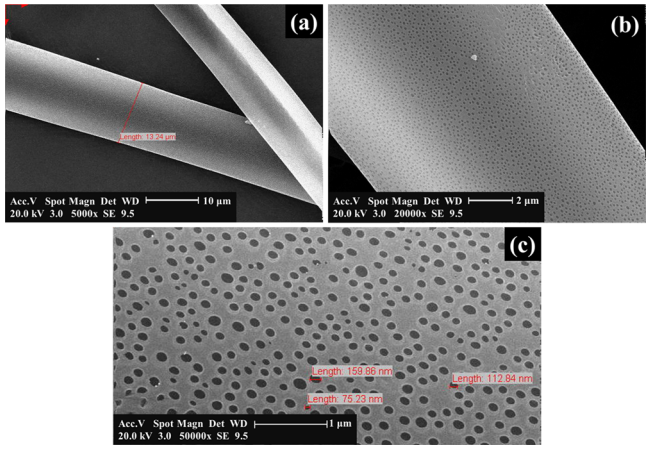

Figure 5. SEM images of PS microfibers with hollow cylindrical nanocavities on the outer surface at different scales (a) 10, (b) 2, and (c) 1 μm.

(Picoquant, GmbH) is used for time-correlated fluorescence lifetime measurements. A pulsed diode laser at the wavelength of 405 nm with a repetition frequency of 10 MHz (LDH-D-C-405 Picoquant, GmbH) as a pulsed excitation source and PDL 800-B laser driver (LD) are employed in our optical setup. Perovskite NWs confined into porous PS microfibers are excited through the lateral surface of the microfiber by a laser beam reflected from the mirror (M). An objective lens (OL) with a numerical aperture of 0.70 (Nikon ELWD 100×) is employed to focus the excitation light reflecting from the dichroic mirror (DM) onto the sample and to collect the fluorescence from the excited NWs. A long pass filter (LPF) with a wavelength of 450 nm is used to completely eliminate the excitation light. A beam splitter (BS) is utilized to split the fluorescence emission from the perovskite NWs onto a CCD Camera, Optronis-1836-ST-153, (CCD) and onto a photo-detector through some linear optical components. A monochromator (MC) is interrogated in the optical setup for tuning emission wavelength from the excited NWs to obtain fluorescence lifetime of the emitters coupled to nanocavities at specific wavelengths. A pinhole (P) with a diameter of 0.75 μm is used to eliminate undesired emissions that are coming apart from the focal plane. A single-photon avalanche diode photodetector (SPAD) is used to detect fluorescence from the excited sample. The decay curves are analyzed using the FluoFit computer program to obtain fluorescence lifetimes; τ_1 and τ_2, amplitude-averaged ($\langle\tau^a\rangle$) and intensity-averaged (τ^b) lifetimes, converging the fitting parameter (χ^2) of the exponential decays to 1. The intensity weighted average lifetime τ^b is defined as

$$\overline{\tau}^b = \frac{\sum_i A_i \tau_i}{\sum_i A_i} \tag{4}$$

and the amplitude weighted average lifetime $\langle\tau^a\rangle$ is given by the following formula

$$\langle\tau^a\rangle = \sum_i \left(\frac{A_i\tau_i}{\sum_i A_i\tau_i}\right)\tau_i \tag{5}$$

where τ_i is the ith component of the fluorescence lifetime, and A_i is its amplitude.

RESULTS AND DISCUSSION

A fluorescence microscopic system (Zeiss) is used to obtain the images of the NWs-doped polymer microfibers. Figure 7 shows the image of two separate microfibers, which include uniformly distributed perovskite NWs. Although the resolution of the images is quite limited for observing the nanocavities, bright individual areas might be attributed to the WGMs of the cylindrical cavities.

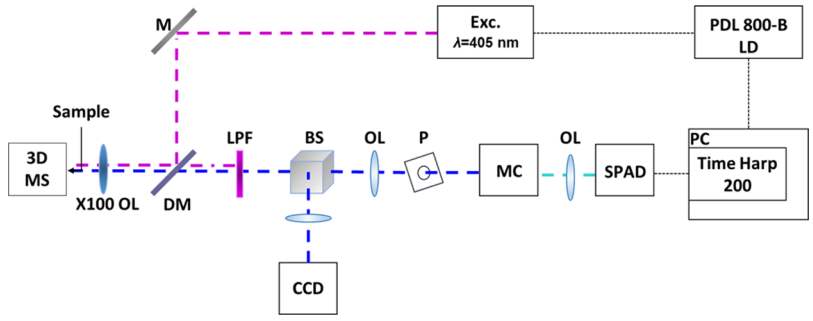

Figure 6. Time-resolved fluorescence lifetime spectroscopy setup

DOI: 10.1021/acs.jpcc.8b12114
J. Phys. Chem. C 2019, 123, 9343−9351

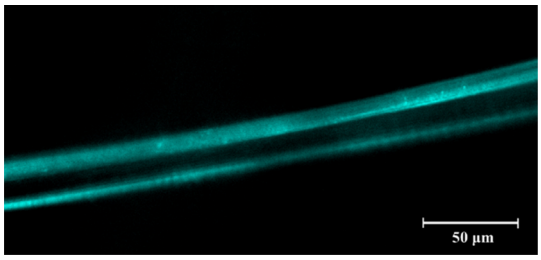

Figure 7. Fluorescence microscopy images of perovskite NWs-doped PS microfibers.

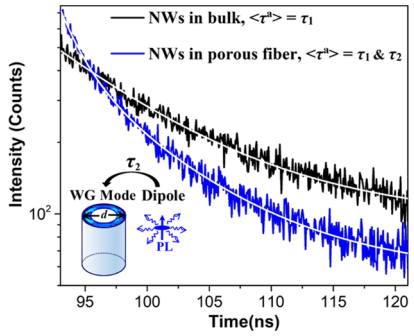

Figure 8. Fluorescence lifetime decay curves of the excited perovskite NWs in the bulk polymer and in a porous microfiber.

The total photoluminescence (PL) emission from the excited NWs originates from the resonant and nonresonant emission. The resonant part corresponds to the coupling of light emission from NWs into the hollow cylindrical nanocavities, which dominates the measured total PL mainly, as seen through its percentage contribution in Table 1. However, some portion of the PL emission, approximately about one-fourth of the total, comes from the nonresonant part, which represents the radiation due to the uncoupled NWs. Fluorescence decay time of the NWs in the bulk polymer is determined to be 21.67 ns, using a single-exponential decay fit. For the NWs embedded in the porous microfiber, a two-exponential decay fit is used to determine the fluorescence lifetime of the emitters, as shown by the white lines in Figure 8. The fluorescence intensity is obtained from the following expression.

$$I = I_1 \exp[-(t - t_0)/\tau_1] + I_2 \exp[-(t - t_0)/\tau_2] \quad (6)$$

In the first part, τ_1 indicates the fluorescence lifetime of the emission coming from the off-resonant NWs, which is considered to be equal to that of the bulk value. In the second term, τ_2 is the average decay time of the light emission from the on-resonant NWs, which is measured to be approximately equal to 4.49 ns. Thus, the average spontaneous emission rate of the perovskite NWs, coupled into the hollow nanocylinders, is observed to enhance by a factor of 4.9, based on our fluorescence time-resolved measurements. The distinctive characteristics of the fluorescence decay curves of the excited NWs in a bulk polymer and a porous microfiber are explicitly seen in Figure 8.

A 3D FDTD method is employed to determine the electric field patterns of the radiating dipoles of the NWs, which are coupled into the cylindrical nanocavities on the surface of a microfiber. The refractive index and the electric field distribution profiles are shown in Figure 9a,b, respectively. In our simulations, hollow nanocavities, which have diameters ranging from 75 to 160 nm, are randomly distributed throughout the surface of the PS microfibers, and the axial axes of these nanostructures are taken to be parallel to the z-axis (see Figures 2 and 9). Magnetic dipoles, which are aligned with the z-axis, are placed near the cavities as indicated by the violet colored points in Figure 9a. As seen in Figure 9b, a number of hollow cylinders, which are located at the borders of the simulation area, owing to the random distribution of the cavities, are not considered in electric field profile. The mesh grid size of the simulations is taken as 3 nm.

As the spot size of the excitation laser beam of 405 nm is about 700 nm after the focusing lens of ×100 OL (see Figure 5), the illuminated area on a single porous microfiber contains approximately 25 hollow cylindrical nanocavities, which are simultaneously excited. However, the WGMs do not appear in all cavities but in very few of them, whose suitable optical properties and physical dimensions match with the spectral range of the NWs and their corresponding resonance wavelengths (see Figure 9b). Thus, the emission from the NWs is localized with different density of electromagnetic states at each excited section of the porous fiber, causing slightly distinctive spontaneous emission rates through the surface of the fiber. The spontaneous rate decay parameters of the emitters, including the percentage values of the fluorescence lifetimes (τ_1 and τ_2) for 11 different regions of the polymer microfiber at specific resonant wavelengths, are given in Table 1. The average fluorescence lifetime of the coupled NWs is measured to be between 3.69 and 5.55 ns for various regions on the porous fiber surface, as presented in Table 1, yielding an average lifetime value of 4.49 ns.

Table 1. Experimental Fluorescence Decay Rate Parameters of Perovskite NWs in Hollow Cylindrical Nanocavities

sample	τ_1 (ns)	τ_1 (%)	τ_2 (ns)	τ_2 (%)	$\langle\tau^a\rangle$ (ns)	τ^b (ns)	χ^2	Γ/Γ_0
bulk	21.67	100					1.05	
region 1	21.70	39.33	5.55	60.67	11.90	17.13	0.99	3.91
region 2	21.67	25.81	4.37	74.19	8.84	15.32	1.04	4.96
region 3	21.41	26.02	4.00	73.98	8.53	15.37	1.00	5.35
region 4	21.76	37.71	4.86	67.29	10.39	16.44	1.05	4.48
region 5	21.51	22.95	4.26	77.05	8.22	14.62	1.02	5.05
region 6	21.55	22.26	4.29	77.74	8.13	14.47	0.94	5.02
region 7	21.66	36.08	4.90	63.92	10.95	16.86	0.97	4.42
region 8	21.52	24.68	4.46	75.32	8.67	14.91	1.04	4.83
region 9	21.61	27.28	4.52	72.72	9.18	15.49	0.98	4.78
region 10	21.56	24.03	4.49	75.97	8.59	14.79	1.01	4.80
region 11	21.56	18.64	3.69	81.36	7.02	13.92	1.06	5.84

DOI: 10.1021/acs.jpcc.8b12114
J. Phys. Chem. C 2019, 123, 9343−9351

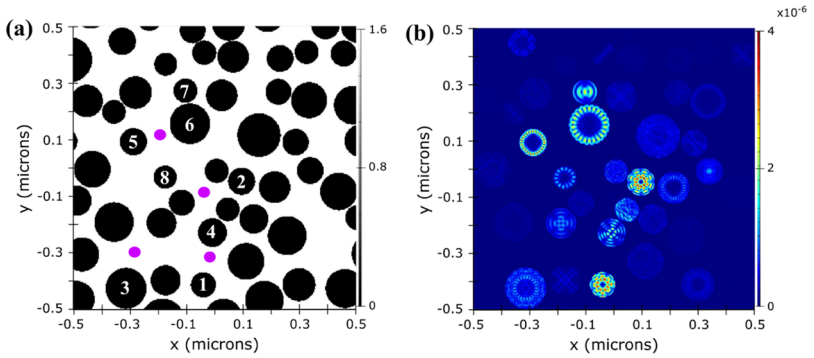

Figure 9. (a) Index profile and (b) electric field distribution of the perovskite NWs coupled into nanocylinders embedded on the surface of a microfiber.

Figure 10 shows the confocal microscope images of the fluorescing perovskite NWs coupled into several hollow nanocavities under pulse excitation, together with a WGM pattern from a single nanocavity only (see Figure 10b), which experimentally confirms that the light coupling into the nanocavities is indeed due to the WGMs. The precision of our instruments is limited for observing the WGMs in each cavity; they rather appear as single bright spots on the surface of the porous microfiber. Nonetheless, a cavity with a slightly larger sized diameter for the nanocylinder seen in Figure 10b enables a clear detection of the WGM possible. Figure 10c shows the fluorescence decay curve of the WGM seen in Figure 10b, whose fast decay is measured to be 3.69 ns, and other related details of this specific WGM are given in Table 1, under the name region 11. It is seen from Table 1 that the experimental data recorded for the single WGM shown in Figure 10b has the highest percentage value for τ_2, implying that the dominant contribution is due to the single WGM; nevertheless, the detected fluorescence also has a contribution from the background signal, which is indicated with τ_1.

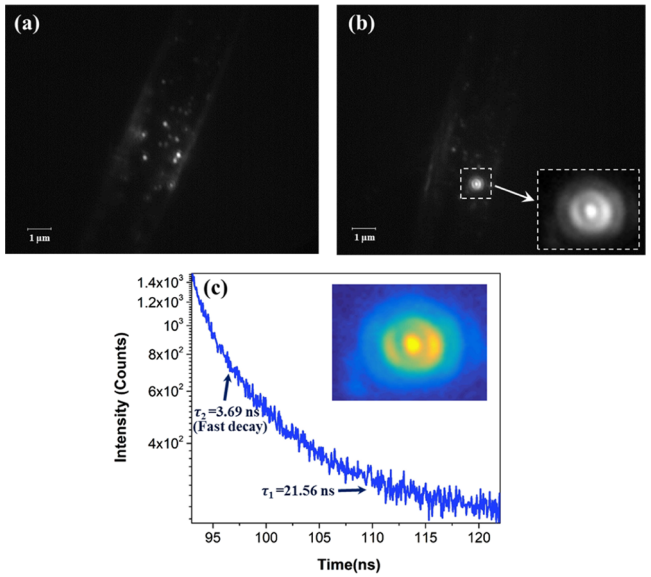

Figure 10. (a) Fluorescence of perovskite NWs coupled into several hollow nanocavities under pulse excitation; (b) WGM pattern from a single nanocavity; inset shows the enlarged image; and (c) fluorescence lifetime characteristics of the WGM shown in part (b), together with its corresponding zoomed and enhanced colored WGM image.

The modification of the spontaneous emission rate of the NWs, coupled to the WGM at specific regions, is also calculated using eq 3. To obtain enhancement factors, the values of the mode volumes are obtained through the FDTD calculations by making use of the resonant wavelengths of the fluorescing emitter for the WGM of the corresponding hollow nanocylinders, which are shown in Figure 9. The mode volume is determined to be 0.032 $(\lambda/n)^3$ for the WGM in nanocavity 1 and 0.072 $(\lambda/n)^3$ for the WGM in nanocylinder 6, which has a larger diameter compared to cavity 1, as shown in Figure 9b. The quality factor of each photonic cavity shown in Figure 9b is also obtained from the FDTD calculations. However, as the linewidth of the perovskite NWs is much broader than the cavity linewidth, a quality factor of approximately 20 is assumed for our photonic nanostructures. Thus, the investigation of the spontaneous emission rate of the encapsulated NWs is assumed to be in a low quality factor regime. Thereupon, the variations in the decay parameters of the coupled NWs at different regions are realized to arise from different values of the mode volumes throughout the surface of the porous microfibers. Calculated enhancement factor, Γ/Γ_0, together with the corresponding quality factor, Q, the mode volume, V, and the hollow cylinder diameter, d, for the determined nanocavities, as described in Figure 9b, are given in Table 2.

Table 2. Theoretical Enhancement Factors, Mode Volumes, and Quality Factors of the Cavities Shown in Figure 9b

cavity	d (nm)	V $(\lambda/n)^3$	Q	Γ/Γ_0
1	88.57	0.032	1228	4.75
2	96.14	0.018	792	8.44
3	144.15	0.070	1886	2.17
4	101.70	0.036	1198	4.22
5	95.96	0.033	1210	4.61
6	142.83	0.072	1504	2.11
7	84.97	0.027	2560	5.63
8	82.07	0.029	1302	5.24

Calculations of the Purcell factor, using eq 1, are reported to be about 10 times greater than the experimental results.[35] On the other hand, eq 3 gives moderately precise results for the distribution of the spontaneous emission rate of the NWs, coupled to the WGM, as this theoretical expression is derived to compensate spatial and spectral mismatches of the dipole

DOI: 10.1021/acs.jpcc.8b12114
J. Phys. Chem. C 2019, 123, 9343−9351

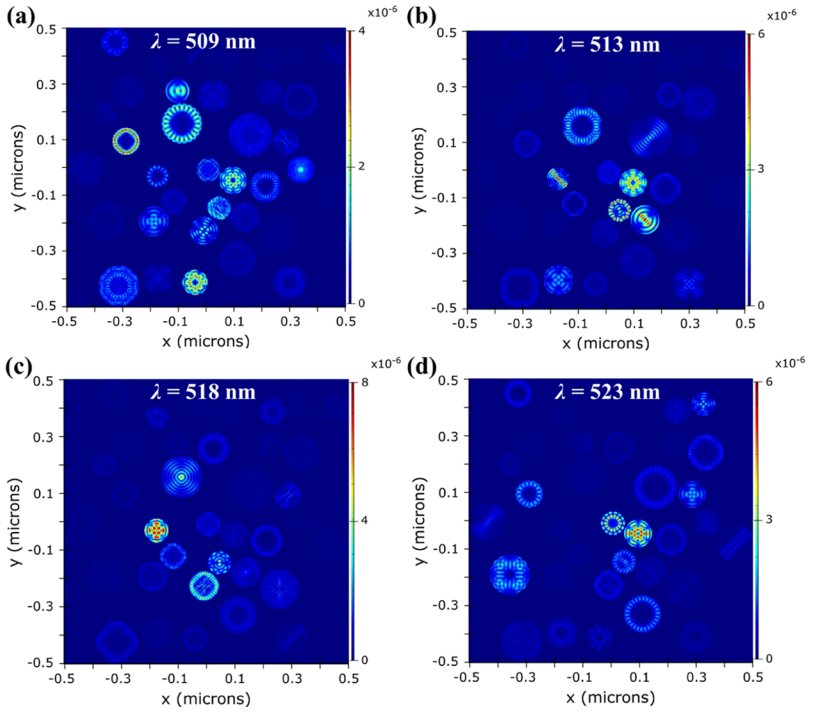

Figure 11. Electric field distributions of the perovskite NWs coupled into hollow cavities on the surface of the microfiber at different resonant wavelengths (a) 509, (b) 513, (c) 518, and (d) 523 nm.

and the cavity mode. For our work here, there is a consistency between theoretical and experimental enhancement values, as given in Tables 1 and 2. In addition to this, in our experiments, all resonant nanostructures in the excited area are taken into consideration to specify the enhancement factor of a specific region, giving an average value of 4.9. Thus, using eq 3, the calculated averaged enhancement value of the resonant cylindrical nanocavities, seen in Figure 9b, is found to be 4.7, clearly confirming that there is a very good agreement between our experimental and theoretical results on the enhancement factor.

Electric field distributions of the dipoles, depicted in Figure 9a, at different resonant wavelengths of 509, 513, 518, and 523 nm, are also presented in Figure 11. Different couplings between dipoles and specific nanocavities at each wavelength are elucidated in simulation pictures (see Figure 11). The theoretical enhancement factor, Γ/Γ_0 is calculated for each resonant wavelength shown in Figure 11, and the results are found to be similar with that of the ones presented in Table 2.

Furthermore, the total fluorescence intensity is also observed to increase, by about 25%, because of the light emission coupled to the WGM, compared to the PL of NWs in the bulk polymer. However, it is not possible to detect the PL spectral signal of the WGMs as the emission from the NWs is collected from various resonant nanostructures in the excited area at the same time. However, the surface morphology of the polymer microfiber may be modified by changing the electrospinning parameters during their production process to allow solely a single nanocavity per spot size of the confocal arrangement.[37] Thus, regularly produced nanostructures on a limited scale through the surface of the PS microfiber allow monitoring a signal in the PL spectrum from only one photonic cavity, using a high-resolution spectrometer. For instance, a similar structure of microtube cavity based on a microchannel glass matrix with a diameter of 8 μm has been reported previously, which allows observing sharp periodic structures in the PL spectrum of the emitters as a result of the confinement of the WGM in one photonic cavity.[38]

Photonic cavities, which support the WGM, have been demonstrated using various structures, which have low mode volumes and high quality factors, resulting in a high Purcell factor. In previous studies, QDs surrounded by microdisks have been widely used to significantly modify spontaneous emission rate of the emitters, coupling to the WGM. A Purcell factor of 190 has been reported for the WGM, which has a quality factor of 12 000 in a microdisk with a diameter of 1.8 μm.[39] Quality factors up to a value of 20 000 have been achieved by cavity modes in larger diameter microdisks.[40] Ultra-high quality factor, small mode volume toroid microcavities on-a-chip have been successfully exhibited by coupling the optical WGM to tapered optical fibers, causing a Purcell factor of 200 000.[41] Coupling the light emission from PbS nanocrystals to the WGM in a Si-based ring resonator as a polymer matrix, with a quality factor of 2500, has been demonstrated for enhancement of the spontaneous emission rate by a factor of 13.[42] Coupling dynamics between graphene and ZnO nanorods have also been well established in a graphene-coated WGM microcavity, using time-resolved experiments.[43] However, manufacturing these highly efficient photonic microcavities requires complex and costly processes. However, in this work, the porous PS matrix, which includes perovskite NWs, presents a stable, reproducible, and a well-designed photonic structure to manipulate the light−matter interactions in hollow cylindrical nanocavities. Highly efficient perovskite nanocrystals offer perfect conditions with their unique optical properties to realize such interactions. Our research here on improving the enhancement spontaneous emission rate of the perovskite NWs, coupled into hollow cylindrical nanocavities on the surface of a microfiber, shows

DOI: 10.1021/acs.jpcc.8b12114
J. Phys. Chem. C 2019, 123, 9343−9351

that such a design is a promising candidate for photonic devices to meaningfully alter the spontaneous emission rate.

CONCLUSIONS

In this paper, fluorescence dynamics of perovskite $CsPbBr_3$ NWs, encapsulated by porous microfibers, are investigated by a time-resolved fluorescence lifetime measurement technique. The possibility of using highly efficient perovskite NWs, uniformly integrated into a PS matrix as a simple, inexpensive optical medium, is investigated through the changes in the spontaneous emission rate of the emitters. As the light emission from the excited NWs is coupled into the hollow nanocylindrical cavities via the WGM, formed on the surface of the polymer fiber, the spontaneous emission rate of the emitters is observed to increase by a factor of 4.9. Our study reveals that using physical and optical properties of such microfibers could be promising for achieving new designs of simple and inexpensive photonic nanocavities to enhance the spontaneous emission rate. These results may provide a significant step toward the comprehension of strong light−matter interactions in polymer-based photonic nanostructures.

AUTHOR INFORMATION

Corresponding Author

*E-mail: naci.inci@boun.edu.tr.

ORCID

Mustafa M. Demir: 0000-0003-1309-3990

M. Naci Inci: 0000-0002-3384-3683

Notes

The authors declare no competing financial interest.

ACKNOWLEDGMENTS

Belkıs Gökbulut acknowledges Boğaziçi University Research Fund for the financial support provided under the contract number 14240.

REFERENCES

(1) Pelton, M. Modified Spontaneous Emission in Nanophotonic Structures. *Nat. Photonics* **2015**, *9*, 427−435.

(2) Tielrooij, K. J.; Orona, L.; Ferrier, A.; Badioli, M.; Navickaite, G.; Coop, S.; Nanot, S.; Kalinic, B.; Cesca, T.; Gaudreau, L.; et al. Electrical Control of Optical Emitter Relaxation Pathways Enabled by Graphene. *Nat. Phys.* **2015**, *11*, 281−287.

(3) Wu, S.; Buckley, S.; Schaibley, J. R.; Feng, L.; Yan, J.; Mandrus, D. G.; Hatami, F.; Yao, W.; Vučković, J.; Majumdar, A.; et al. Monolayer Semiconductor Nanocavity Lasers with Ultralow Thresholds. *Nature* **2015**, *520*, 69−72.

(4) Claudon, J.; Bleuse, J.; Malik, N. S.; Bazin, M.; Jaffrennou, P.; Gregersen, N.; Sauvan, C.; Lalanne, P.; Gérard, J.-M. A Highly Efficient Single-Photon Source Based on a Quantum Dot in a Photonic Nanowire. *Nat. Photonics* **2010**, *4*, 174−177.

(5) Polman, A.; Atwater, H. A. Photonic Design Principles for Ultrahigh-Efficiency Photovoltaics. *Nat. Mater.* **2012**, *11*, 174−177.

(6) Lu, D.; Kan, J. J.; Fullerton, E. E.; Liu, Z. Enhancing Spontaneous Emission Rates of Molecules Using Nanopatterned Multilayer Hyperbolic Metamaterials. *Nat. Nanotechnol.* **2014**, *9*, 48−53.

(7) Hoang, T. B.; Akselrod, G. M.; Argyropoulos, C.; Huang, J.; Smith, D. R.; Mikkelsen, M. H. Ultrafast Spontaneous Emission Source Using Plasmonic Nanoantennas. *Nat. Commun.* **2015**, *6*, 7788.

(8) Galfsky, T.; Sun, Z.; Considine, C. R.; Chou, C.-T.; Ko, W.-C.; Lee, Y.-H.; Narimanov, E. E.; Menon, V. M. Broadband Enhancement of Spontaneous Emission in Two-Dimensional Semiconductors Using Photonic Hypercrystals. *Nano Lett.* **2016**, *16*, 4940−4945.

(9) Tsakmakidis, K. L.; Boyd, R. W.; Yablonovitch, E.; Zhang, X. Large spontaneous-emission enhancements in metallic nanostructures: towards LEDs faster than lasers. *Opt. Express* **2016**, *24*, 17916−17927.

(10) Russel, K. J.; Liu, T. L.; Cui, S.; Hu, E. L. Large Spontaneous Emission Enhancement in Plasmonic Nanocavities. *Nat. Photonics* **2012**, *6*, 459−462.

(11) Bulgarini, G.; Reimer, M. E.; Zehender, T.; Hocevar, M.; Bakkers, E. P. A. M.; Kouwenhoven, L. P.; Zwiller, V. Spontaneous Emission Control of Single Quantum Dots in Bottom-Up Nanowire Waveguides. *Appl. Phys. Lett.* **2012**, *100*, 121106.

(12) Birowosuto, M. D.; Zhang, G.; Yokoo, A.; Takiguchi, M.; Notomi, M. Spontaneous Emission Inhibition of Telecom-Band Quantum Disks Inside Single Nanowire on Different Substrates. *Opt. Express* **2014**, *22*, 11713−11726.

(13) Gökbulut, B.; Inci, M. N. Inhibition of Spontaneous Emission in a Leaky Mode Wedge Nanocavity. *Photonics Nanostructures: Fundam. Appl.* **2018**, *32*, 68−73.

(14) Lohrmann, A.; Karle, T. J.; Sewani, V. K.; Laucht, A.; Bosi, M.; Negri, M.; Castelletto, S.; Prawer, S.; McCallum, J. C. Integration of Single Photon Emitters into 3C-SiC Microdisk Resonators. *ACS Photonics* **2017**, *4*, 462−468.

(15) Javerzac-Galy, C.; Kumar, A.; Schilling, R. D.; Piro, N.; Khorasani, S.; Barbone, M.; Goykhman, I.; Khurgin, J. B.; Ferrari, A. C.; Kippenberg, T. J. Excitonic Emission of Monolayer Semiconductors Near-Field Coupled to High-Q Microresonators. *Nano Lett.* **2018**, *18*, 3138−3146.

(16) Noda, S.; Fujita, M.; Asano, T. Spontaneous-Emission Control by Photonic Crystals and Nanocavities. *Nat. Photonics* **2007**, *1*, 449−458.

(17) Jakubczyk, T.; Franke, H.; Smoleński, T.; Ściesiek, M.; Pacuski, W.; Golnik, A.; Schmidt-Grund, R.; Grundmann, M.; Kruse, C.; Hommel, D.; et al. Inhibition and Enhancement of the Spontaneous Emission of Quantum Dots in Micropillar Cavities with Radial-Distributed Bragg Reflectors. *ACS Nano* **2014**, *8*, 9970−9978.

(18) Gökbulut, B.; Yartaşı, E.; Sunar, E.; Kalaoglu-Altan, O. I.; Gevrek, T. N.; Sanyal, A.; Inci, M. N. Humidity Induced Inhibition and Enhancement of Spontaneous Emission of Dye molecules in a Single PEG Nanofiber. *Opt. Mater. Express.* **2018**, *8*, 568−580.

(19) Li, X.; Cao, F.; Yu, D.; Chen, J.; Sun, Z.; Shen, Y.; Zhu, Y.; Wang, L.; Wei, Y.; Wu, Y. All Inorganic Halide Perovskites Nanosystem: Synthesis, Structural Features, Optical Properties and Optoelectronic Applications. *Small* **2017**, *13*, 1603996.

(20) Bi, D.; Tress, W.; Dar, M. I.; Gao, P.; Luo, J.; Renevier, C.; Schenk, K.; Abate, A.; Giordano, F.; Baena, J. P. C. Efficient Luminescent Solar Cells Based on Tailored Mixed-Cation Perovskites. *Sci. Adv.* **2016**, *2*, No. e1501170.

(21) Beal, R. E.; Slotcavage, D. J.; Leijtens, T.; Bowring, A. R.; Belisle, R. A.; Nguyen, W. H.; Burkhard, G. F.; Hoke, E. T.; McGehee, M. D. Cesium Lead Halide Perovskites with Improved Stability for Tandem Solar Cells. *J. Phys. Chem. Lett.* **2016**, *7*, 746−751.

(22) Nedelcu, G.; Protesescu, L.; Yakunin, S.; Bodnarchuk, M. I.; Grotevent, M. J.; Kovalenko, M. V. Fast Anion-Exchange in Highly Luminescent Nanocrystals of Cesium Lead Halide Perovskites (CsPbX3, X = Cl, Br, I). *Nano Lett.* **2015**, *15*, 5635−5640.

(23) Akbali, B.; Topcu, G.; Guner, T.; Ozcan, M.; Demir, M. M.; Sahin, H. CsPbBr3 Perovskites: Theoretical and Experimental Investigation on Water-Assisted Transition from Nanowire Formation to Degradation. *Phys. Rev. Mater.* **2018**, *2*, 034601.

(24) Amgar, D.; Stern, A.; Rotem, D.; Porath, D.; Etgar, L. Tunable Length and Optical Properties of CsPbX3 (X = Cl, Br, I) Nanowires with a Few Unit Cells. *Nano Lett.* **2017**, *17*, 1007−1013.

(25) Etgar, L. The merit of perovskite's dimensionality; can this replace the 3D halide perovskite? *Energy Environ. Sci.* **2018**, *11*, 234−242.

(26) Shoaib, M.; Zhang, X.; Wang, X.; Zhou, H.; Xu, T.; Wang, X.; Hu, X.; Liu, H.; Fan, X.; Zheng, W.; et al. Directional Growth of Ultralong CsPbBr3 Perovskite Nanowires for High-Performance Photodetectors. *J. Am. Chem. Soc.* **2017**, *139*, 15592−15595.

DOI: 10.1021/acs.jpcc.8b12114
J. Phys. Chem. C 2019, 123, 9343−9351

(27) Wang, X.; Shoaib, M.; Wang, X.; Zhang, X.; He, M.; Luo, Z.; Zheng, W.; Li, H.; Yang, T.; Zhu, X.; et al. High-Quality In-Plane Aligned CsPbX3 Perovskite Nanowire Lasers with Composition-Dependent Strong Exciton-Photon Coupling. *ACS Nano* **2018**, *12*, 6170−6178.
(28) Wang, X.; Zhou, H.; Yuan, S.; Zheng, W.; Jiang, Y.; Zhuang, X.; Liu, H.; Zhang, Q.; Zhu, X.; Wang, X.; et al. Cesium lead halide perovskite triangular nanorods as high-gain medium and effective cavities for multiphoton-pumped lasing. *Nano Res.* **2017**, *10*, 3385−3395.
(29) Li, G.; Rivarola, F. W. R.; Davis, N. J. L. K.; Bai, S.; Jellicoe, T. C.; de la Peña, F.; Hou, S.; Ducati, C.; Gao, F.; Friend, R. H. Highly Efficient Perovskite Nanocrystal Light-Emitting Diodes Enabled by a Universal Crosslinking Method. *Adv. Mater.* **2016**, *28*, 3528−3534.
(30) Deschler, F.; Price, M.; Pathak, S.; Klintberg, L. E.; Jarausch, D.-D.; Higler, R.; Hüttner, S.; Leijtens, T.; Stranks, S. D.; Snaith, H. J. High Photoluminescence Efficiency and Optically Pumped Lasing in Solution-Processed Mixed Halide Perovskite Semiconductors. *J. Phys. Chem. Lett.* **2014**, *5*, 1421−1426.
(31) Purcell, E. M. Spontaneous Emission Probabilities at Radio Frequencies. *Phys. Rev.* **1946**, *69*, 681.
(32) Romeira, B.; Fiore, A. Purcell Effect in the Stimulated and Spontaneous Emission Rates of Nanoscale Semiconductor Lasers. *IEEE J. Quantum Electron.* **2018**, *54*, 2000412.
(33) Gérard, J.; Sermage, B.; Gayral, B.; Legrand, B.; Costard, E.; Thierry-Mieg, V. Enhanced Spontaneous Emission by Quantum Boxes in a Monolithic Optical Microcavity. *Phys. Rev. Lett.* **1998**, *81*, 1110−1113.
(34) Gerard, J.-M.; Gayral, B. Strong Purcell Effect for InAs Quantum Boxes in Three-Dimensional Solid-State Microcavities. *J. Lightwave Technol.* **1999**, *17*, 2089−2095.
(35) Solomon, G. S.; Xie, Z.; Fang, W.; Xu, J. Y.; Yamilov, A.; Cao, H.; Ma, Y.; Ho, S. T. Large Spontaneous Emission Enhancement in InAs Quantum Dots Coupled to Microdisk Whispering Gallery Modes. *Phys. Status Solidi B* **2003**, *238*, 309−312.
(36) Isık, T.; Demir, M. M. Tailored Electrospun Fibers from Waste Polystyrene for High Oil Adsorption. *Sustainable Mater. Technol.* **2018**, *18*, No. e00084.
(37) Casper, C. L.; Stephens, J. S.; Tassi, N. G.; Chase, D. B.; Rabolt, J. F. Controlling Surface Morphology of Electrospun Polystyrene Fibers: Effect of Humidity and Molecular Weight in the Electrospinning Process. *Macromolecules* **2004**, *37*, 573−578.
(38) Rusakov, K. I.; Gladyshchuk, A. A.; Rakovich, Y. P.; Donegan, J. F.; Balakrishnan, S.; Gun'ko, Y.; Perova, T. S.; Moore, R. A. Whispering gallery mode emission from microtube cavity. *Opt. Spectrosc.* **2007**, *103*, 360−365.
(39) Gayral, B.; Gérard, J. M.; Lemaître, A.; Dupuis, C.; Manin, L.; Pelouard, J. L. High-Q Wet-Etched GaAs Microdisks Containing InAs Quantum Boxes. *Appl. Phys. Lett.* **1999**, *75*, 1908−1910.
(40) Michler, P.; Kiraz, A.; Zhang, L.; Becher, C.; Hu, E.; Imamoglu, A. Laser Emission from Quantum Dots in Microdisk Structures. *Appl. Phys. Lett.* **2000**, *77*, 184−186.
(41) Kippenberg, T. J.; Spillane, S. M.; Vahala, K. J. Demonstration of ultra-high-Q small mode volume toroid microcavities on a chip. *Appl. Phys. Lett.* **2004**, *85*, 6113−6115.
(42) Humer, M.; Guider, R.; Jantsch, W.; Fromherz, T. Integration, Photostability and Spontaneous Emission Rate Enhancement of Colloidal PbS Nanocrystals for Si-Based Photonics at Telecom Wavelengths. *Opt. Express* **2013**, *21*, 18680−18688.
(43) Li, J.; Xu, C.; Nan, H.; Jiang, M.; Gao, G.; Lin, Y.; Dai, J.; Zhu, G.; Ni, Z.; Wang, S.; et al. Graphene Surface Plasmon Induced Optical Field Confinement and Lasing Enhancement in ZnO Whispering-Gallery Microcavity. *ACS Appl. Mater. Interfaces* **2014**, *6*, 10469−10475.

DOI: 10.1021/acs.jpcc.8b12114
J. Phys. Chem. C 2019, 123, 9343−9351